JOURNAL OF MATERIALS SCIENCE **36** (2001) 5101 – 5104

Development of nanocrystals in an amorphous alloy $Zr_{47}Ni_{30}Ti_{23}$

S. YI
Reliability Assessment Center for Metallic Materials, Korea Institute of Industrial Technology, Chonan, Korea
E-mail: shyi@kitech.re.kr

W. T. KIM, D. H. KIM
Center for Noncrystalline Materials, Department of Metallurgical Engineering, Yonsei University, Seoul, Korea

S. H. OH, C. G. PARK
Department of Materials Science and Engineering, Pohang University of Science and Technology, Pohang, Korea

Development of nanocrystals during crystallization of an amorphous alloy $Zr_{47}Ni_{30}Ti_{23}$ is studied using differential scanning calorimetry (DSC), X-ray diffraction (XRD) and high resolution transmission electron microscopy (HRTEM). Up on heating the amorphous ribbon in DSC, three exothermic peaks including a broad peak are observed. Stable nanocrystals embedded in the amorphous matrix form through primary crystallization. The nanocrystals have uniform sizes after prolonged annealing at 400°C for 180 minutes. Ni plays an important role for the stability of the nanocrystals. Due to the Ni partitioning between the nanocrystals and the residual matrix, the crystallization temperature (T_{xl}) of the residual amorphous matrix increases as crystallization proceeds. The formation of nanocrystal-amorphous composites that have high microstructural stability is possible through the controlled crystallization of the amorphous alloy $Zr_{47}Ni_{30}Ti_{23}$.
© *2001 Kluwer Academic Publishers*

1. Introduction

Crystallization of amorphous materials is an effective way to produce nanocrystal-amorphous composites (NAC) in which nanocrystals are dispersed in the amorphous phase matrix. Fully dense NAC can be fabricated through the controlled crystallization of an amorphous phase [1]. Many NAC have enhanced mechanical/physical properties. For instance, the tensile strength of an A1 based, partially crystallized amorphous ribbon has been found to be increased up to 1550 MPa [2]. Recently, mechanical properties of Zr-based bulk amorphous alloys have been improved by nanocrystal precipitation in the amorphous matrix [3, 4].

Two mechanisms have been proposed for the formation of nanocrystals embedded in the amorphous matrix. One of the two mechanisms includes phase separation by a spinodal decomposition as a necessary precursor before crystallization. Following the phase separation, nanocrystals develop in the region that has a lower crystallization temperature (T_x). Therefore, nanocrystals are uniformly distributed and the maximum size of nanocrystals is limited to the length scale of the spinodal decomposition domain. The other mechanism assumes the primary crystallization of nanocrystals in the supercooled liquid region. As the nucleated grains grow, compositional gradients around the grains develop. The residual amorphous phase around the grain is stabilized by the compositional change. That is, the resistance of the residual amorphous phase against further crystallization increases. Therefore, the grain growth rate is significantly retarded as crystallization proceeds, resulting in the formation of nanocrystals embedded in the stable amorphous matrix at a certain annealing temperature. Nanocrystals formed by this mechanism are randomly distributed in the amorphous matrix.

In some Zr-based bulk amorphous alloys, nanocrystal formation attributed to a spinodal decomposition in the supercooled liquid has been reported [5–8]. However, it has been also reported that the transition from phase separation to non-phase separation can be occurred by a small compositional change in the Zr-based bulk amorphous alloys [8]. In this study, formation of nanocrystals in an amorphous ribbon of the alloy $Zr_{47}Ni_{30}Ti_{23}$ is studied to give an insight on the nanocrystal formations in the Zr-based multi-component bulk amorphous alloys.

2. Experimental

A 30 g ingot of the $Zr_{47}Ni_{30}Ti_{23}$ alloy was prepared by arc-melting using high purity elements; Ti : 99.95%, Zr : 99.8, Ni : 99.95. An amorphous ribbon was prepared by a melt spinning method with the wheel surface velocity ~30 m/s. Crystallization behaviors of the amorphous ribbon were studied by a differential scanning calorimetry (DSC, Perkin-Elmer DSC 7) with the heating/cooling rates ranging 20°C–40°C/min under an Ar atmosphere. The structures and morphologies of the crystalline phases were identified by X-ray diffraction (XRD) and transmission electron microscopy (TEM) analysis. The X-ray diffraction measurements were made by Rigaku CN2301 using Cu K_α radiation. The observation of high resolution TEM (HRTEM) was carried out using field emission-TEM (FE-TEM; JEOL, JEM2010F) operating at 200 kV. Thin foil specimen for TEM observation was prepared by dimpling, followed by Ar-ion milling using a precision ion polishing system (PIPS; Gatan, Model 691) at 4 kV at an angle of 6°.

3. Results

The alloy composition locates near the pseudo-binary eutectic point between Laves phase and Zr_2Ni phase as shown in Fig. 1 [9]. Equilibrium phases in the alloy $Zr_{47}Ni_{30}Ti_{23}$ are mainly Laves phase and Zr_2Ni phase, and a small amount of α-Zr(Ti) solid solution. During rapid quenching in the melt spinner, formation of the crystalline phases from liquid is completely suppressed as can be confirmed by XRD and TEM analysis. DSC heating curve of the as-melt spun ribbon has three exothermic peaks including one broad peak with the onset temperature $T_{x1} = 363$°C and the peak temperature $T_{p1} = 395$°C as shown in Fig. 2a. The occurrence of three exothermic events indicates at least three step crystallization of the $Zr_{47}Ni_{30}Ti_{23}$ amorphous ribbon. Fig. 3 shows XRD spectra of the annealed ribbons at several temperatures. Sharp peaks attributed to the formation of crystalline phases are not detected in the ribbons annealed at temperatures below 445°C. However, as the annealing temperature increases, the broad peak becomes narrower and the peak position shifts to a higher degree as shown in Fig. 3a. In the XRD pattern of the ribbon annealed at 500°C, some diffraction peaks superimposed onto a broad hallo pattern can be resolved. Since the diffraction peaks can not be indexed by any phase reported in the alloy composition range of the ternary system Zr-Ni-Ti, the diffraction peaks are marked as unidentified peaks in Fig. 3b. In the XRD pattern of the ribbon annealed at the peak temperature of the second exothermic event (524°C), diffraction peaks corresponding to the ZrTiNi Laves phase can be observed. Finally, Zr_2Ni phase can be identified in the XRD pattern obtained from the fully crystallized ribbon.

Although the DSC trace of the as-melt spun ribbon clearly shows a reaction around 400°C, crystalline

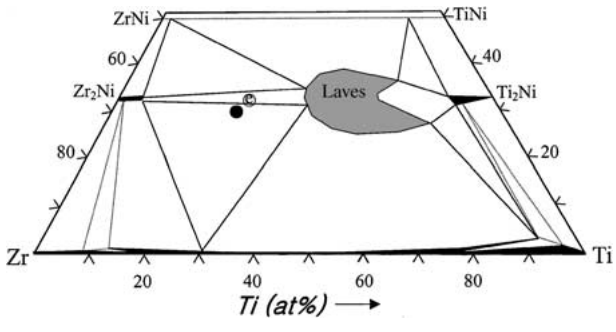

Figure 1 A partial isothermal section of the Zr-Ni-Ti ternary system at 700°C (after Eremenko *et al.* [9]). ⓒ and ● represent the pseudo-binary eutectic and the alloy composition $Zr_{47}Ni_{30}Ti_{23}$, respectively.

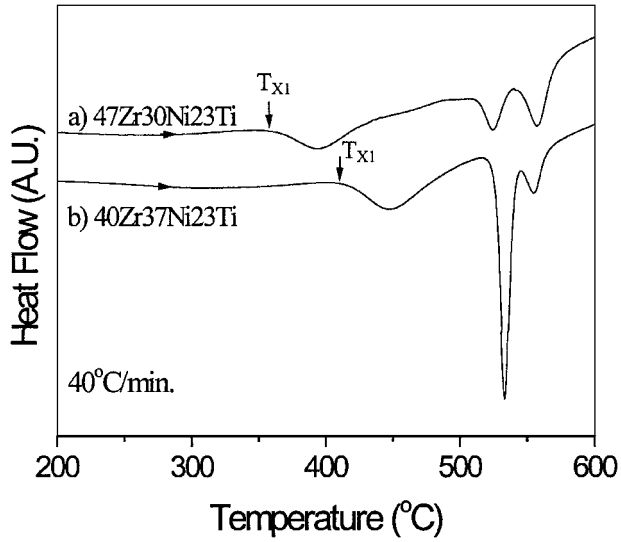

Figure 2 DSC heating curves showing three exothermic peaks. The onset temperature of the first exothermic event shifts to a higher temperature as Ni content increases.

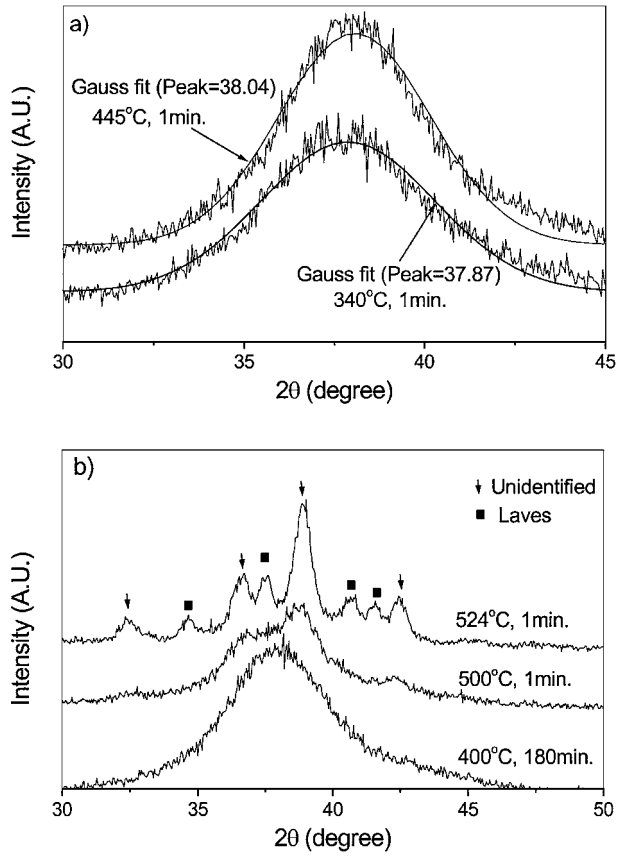

Figure 3 (a) X-ray spectra of partially crystallized ribbons around the peak temperature of the first exothermic event showing the peak shifts to a higher degree as crystallization proceeds. (b) X-ray spectra of partially crystallized ribbons.

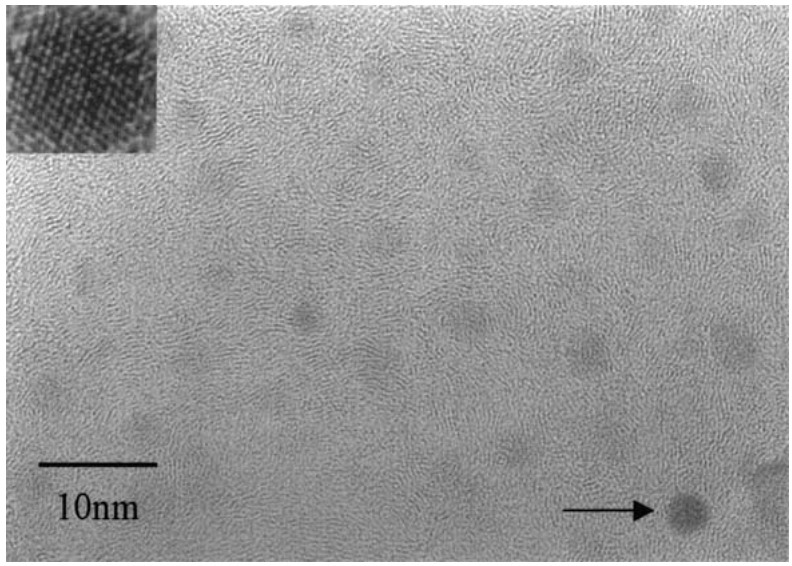

Figure 4 HRTEM image of the ribbon annealed at 400°C for 180 minutes showing nanocrystals embedded in the amorphous matrix. Inset is the magnified image of the grain marked by arrow.

phases can not be detected in the XRD spectra of the ribbon annealed at 445°C. The crystalline phase formed during the first exothermic event may be too fine to be detected by XRD. Even after a prolonged annealing treatment at 400°C for 180 minutes, sharp peaks attributed to the formation of crystalline phases cannot be resolved in the XRD spectra (Fig. 3b). However, a careful examination of the annealed ribbon in HRTEM reveals nanocrystals embedded in the amorphous matrix (Fig. 4). The nanocrystals are randomly distributed in the amorphous matrix. A regularly spaced lattice fringe image is observed in the grain marked by the arrow in Fig. 4. Dislocations are not observed in the nanocrystal even though lattice distortion is observed as shown in the inset. During the second exothermic event, Laves phase forms as identified by the XRD spectra of the ribbon annealed at the second exothermic peak temperature, 524°C (Fig. 3).

Upon re-heating of the ribbons annealed at 400°C, the higher peak temperature of the first exothermic event than that of as-melt spun ribbon is observed in the DSC heating curve. However, the peak temperatures of the second and third exothermic events are not changed (Fig. 5a–c) unless the reaction corresponding to the second exothermic event occurs. Once the reaction corresponding to the second exothermic event occurs during annealing, the second and third exothermic peak temperatures shift to lower temperatures upon re-heating of the annealed sample (Fig. 5d).

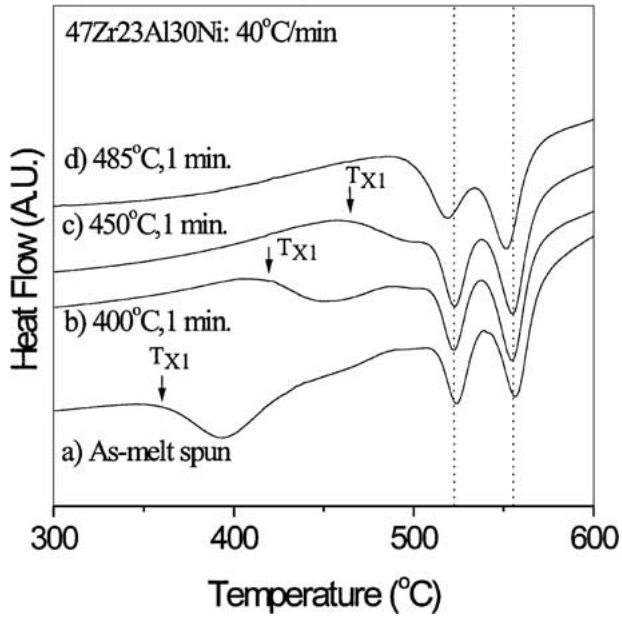

Figure 5 DSC heating curves of the as-melt spun ribbon and the annealed ribbons.

4. Discussion

The existence of very fine, randomly distributed, nanocrystals (<5 nm) even after the prolonged annealing treatment at around first peak temperature indicates the sluggish growth kinetics of the nucleated crystals. The sluggish growth kinetics is attributed to the enhanced resistance of the remained amorphous matrix against crystallization. The random distribution of nanocrystals in the amorphous matrix may be attributed to the formation of nanocrystals by quenched-in nuclei.

A narrow size distribution of nanocrystals obtained from HRTEM images also indicates that growth kinetics is retarded as crystallization proceeds. That is, in the early stage of annealing treatment, a number of nanocrystals nucleates and grows relatively fast. However, as crystallization proceeds during annealing, growth rates are retarded since the residual amorphous phases around the crystals are stabilized by the compositional change. Since the nanocrystal size is not large enough for the compositional analysis in TEM, the compositional change in the amorphous matrix after the annealing treatment can not be directly detected. However, the XRD spectra of partially crystallized ribbons strongly indicate that Ni is enriched in the residual amorphous matrix as crystallization corresponding to the first exothermic event proceeds. That is, the broad peak positions obtained from the ribbons annealed at

340°C and 445°C shift to higher degrees than that obtained form the as-melt spun ribbon (Fig. 3). These peak position shifts imply that the content of the small sized element, Ni, in the amorphous phase increases through the partial crystallization. Therefore, as the nanocrystals grow, more Ni is rejected to the supercooled liquid region around the nanocrystals, increasing the Ni content in the residual amorphous phase. In the Zr-Ni binary system, the amorphous phase having higher Ni content is more stable. That is, the T_x of the supercooled liquid phase increases with the increase of Ni content [10]. Similar effects of Ni content on the T_{x1} of the amorphous phase in the Zr-Ni-Ti ternary system is confirmed from the DSC trace of the amorphous ribbon of the alloy $Zr_{40}Ni_{37}Ti_{23}$. As shown in Fig. 2b, the T_{x1} of the high Ni content alloy $Zr_{40}Ni_{37}Ti_{23}$ is higher than that of the low Ni content alloy $Zr_{47}Ni_{30}Ti_{23}$ (Fig. 2b). Therefore, it is concluded that as crystallization proceeds, the T_{x1} of the residual amorphous phase increases due to Ni re-distribution between the nanocrystals and the residual amorphous phase around the nanocrystals. The increase in the T_{x1} leads to the formation of nanocrystals that are very stable during the isothermal annealing treatment. During the isothermal annealing at a certain temperature higher than the T_{x1} of as-melt spun ribbon, nanocrystals randomly nucleate and grow relatively fast. However, as crystallization proceeds, the T_{x1} of the residual amorphous phase continuously increases. When the T_{x1} of the residual amorphous phase is higher than the annealing temperature, crystallization kinetics is significantly retarded and thus nanocrystals are stabilized even after prolonged isothermal annealing treatment.

Since the Laves phase that forms during second exothermic event has higher Ni content than the alloy composition $Zr_{47}Ni_{30}Ti_{23}$, Ni is depleted in the amorphous phase surrounding the Laves phases leading to the decrease of the onset temperature of the second exothermic event, T_{x2}. The decreased T_{x2} is observed during re-heating of the partially crystallized ribbon at 485°C that has Laves grains (Fig. 5d). Since the T_{x2} decreases as crystallization corresponding to the second exothermic event proceeds, the Laves grains grow fast during isothermal annealing until the grain is impinged against adjacent grains.

5. Conclusion

Fully amorphous phase can be formed in the alloy $Zr_{47}Ni_{30}Ti_{23}$ by a melt spinning method. The amorphous phase crystallize in three steps during continuous heating. Nanocrystals embedded in the amorphous matrix form during annealing at around the peak temperature of the first exothermic event (395°C). A very narrow size distribution of the nanocrystals is obtained from the HRTEM images of the ribbons annealed at 400°C for 180 minutes. The nanocrystals are very stable even after prolonged annealing treatment at around first peak temperature. Based upon XRD and DSC results, it is inferred that nanocrystals form via primary crystallization during the first exothermic event. As the primary crystallization proceeds, Ni is more enriched in the residual amorphous phase leading to the continuous increase in the T_{x1}. Due to the increase in the T_{x1} of the residual amorphous phase, the crystallization kinetics is retarded inhibiting the growth of nanocrystals during isothermal annealing. However, the Laves phase crystallization during the second exothermic event results in the depletion of Ni in the amorphous phase surrounding the Laves phase. The T_{x2} decreases as the crystallization proceeds leading to the rapid grain growth of Laves phase grains. Therefore, it is concluded that Ni can play an important role for the stabilization of nanocrystals in the amorphous alloy $Zr_{47}Ni_{30}Ti_{23}$. The NAC materials that have excellent microstructural stability can be fabricated by the controlled crystallization of the amorphous alloy $Zr_{47}Ni_{30}Ti_{23}$.

Acknowledgement

This work was supported by Creative Research Initiatives of the Korean Ministry of Science and Technology.

References

1. K. LU, R. LÜCK and B. PREDEL, *Mater. Sci. Eng.* **A179/180** (1994) 536.
2. T. MASUMOTO, *ibid.* **A179/180** (1994) 8.
3. L. Q. XING, J. ECKERT, W. LÖSER and L. SCHULTZ, *Appl. Phys. Lett.* **74**(5) (1999) 664.
4. C. FAN, A. TAKEUCHI and A. INOUE, *Mater. Trans. JIM* **40**(1) (1999) 42.
5. S. SCHNEIDER, P. THIYAGARAJAN and W. L. JOHNSON, *Appl. Phys. Lett.* **68**(4) (1996) 493.
6. L. Q. XING, G. P. GÖRLER and D. M. HERLACH, *Mater. Sci. Eng.* **A226–228** (1997) 429.
7. T. A. WANIUK, R. BUSCH, A. MASUHR and W. L. JOHNSON, *Acta Mater.* **46**(15) (1998) 5229.
8. C. C. HAYS, C. P. KIM and W. L. JOHNSON, *Appl. Phy. Lett.* **75**(8) (1999) 1089.
9. P. VILLAS, A. PRINCE and H. OKAMOTO (Eds), "Handbook of Tenary Alloy Phase Diagrams" (ASM International, Materials Parks, OH) p. 13063.
10. Y. D. DONG, G. GREGAN and M. G. SCOTT, *J. Non-Cryst. Solids.* **43** (1981) 403.

Received 1 December 2000
and accepted 26 June 2001